Multimedia Tools and Applications (2021) 80:16441–16472
https://doi.org/10.1007/s11042-020-09913-3

On the local behavior of spaces of range image patches

Jinhong Li[1] · **Shengxiang Xia**[2]

Received: 10 July 2019 / Revised: 20 June 2020 / Accepted: 16 September 2020 /
Published online: 30 October 2020

Abstract
We focus on the quantitative and local topological properties of range images. We consider the spaces M_m of $m \times m$ high-contrast patches of range images for m=3, 5, 7, 9, 11. Using computational topological tools to analyze range image patches, we detect that M_3 (M_9, M_{11}) has core subsets with the topology of a circle, M_3, M_5, M_7, M_9 and that M_{11} have some subspaces with the topology of a Klein bottle. We also discover that the largest subspace with the Klein bottle's topology decreases as the measurements of patches increase, which generalizes the results in the paper of H. Adams and G. Carlsson, and demonstrates properties among optical images and range image patches, which are more similar than those established by Lee et al.

Keywords Range images · Topology · Persistent homology · Klein bottle · Barcode

1 Introduction

Range images have attracted an increasing amount of interest in recent years for two reasons: First, they can be employed in various industrial applications [13, 17]; second, more practical models of optical images can be built by using a range image [4, 14]. Every range image can be considered to be a very high-dimensional vector of a space $\mathcal{P}$. When we directly study a set of images $\mathcal{G} \subseteq \mathcal{P}$, we encounter the high-dimensional problem of $\mathcal{G}$ and the sparsity of $\mathcal{G}$ in $\mathcal{P}$. One approach is to analyze the state space of local patterns of pixel values, which are modeled by small patches of images. Reducing the dimension of the problem is one advantage of locally analyzing a range image space, and another advantage (suggested by Field [9] and Hateren [22]) is that many global statistical properties of

✉ Shengxiang Xia
xias@sdjzu.edu.cn

Jinhong Li
lijinhong@qlu.edu.cn

[1] School of Mathematics and Statistics, Qilu University of Technology, Jinan, 250353, People's Republic of China

[2] School of Science, Shandong Jianzhu University, Jinan, 250101, People's Republic of China

the space can be provided by local statistics. The authors of [15] present several interesting observations about the resulting spaces of optical and range images 3×3 patches; for example, they discover that most of the optical 3×3 high-contrast patches are concentrated around a 2-dimensional loop. In [6], Carlsson et al. analyzed optical patches (studied by Lee et al. [15]) by using computational topological tools; they find that there is a large 2-dimensional subset with the same homology as a Klein bottle. The authors establish a relation between the optical patch space and the 2-variable polynomials and applied it to prove the existence of a subspace of the optical patch space with a topology that resembles that of a Klein bottle.

In [2], the authors revealed that 5×5 and 7×7 range image patches possess the topology of a circle.

In this study, we utilize the methods of [2] to range patches and describe the global topological structure of various sizes of range image patches. In particular, we show that there is a 2-dimensional subset of M_3, M_5, M_7, M_9 and M_{11} with the homology of a Klein bottle, which can improve the image compression technique [6]. The results of this paper show that optical patches and range patches have very similar properties.

The main contributions of this paper are listed as follows:

- We theoretically prove that there exists a subspace in spheres S^n which is homeomorphic to a Klein bottle, and describe a method to construct a approximation of the Klein bottle in S^n ($n = 8, 24, 48, 80, 120$). Furthermore, by the approximation of the Klein bottle in S^n, we show that there is a subspace of high-contrast 3×3 (5×5, 7×7, 9×9 and 11×11) range patches with homology of a Klein bottle.
- We demonstrate that the sizes of the largest subspaces of range patches M_3, M_5, M_7, M_9, and M_{11} with the Klein bottle's topology decrease with the increasing measurement of range patches; moreover, the Klein bottle behavior of the range patches gradually disappears as the size of range patches increases (Table 1).
- We demonstrate that there is a subspace of the spaces of 9×9 (11×11) range patches that has circular behavior.

2 From point clouds to complexes

For a sampled subset S of a space X, to estimate the topological construction of X, we usually create a simplicial complex K by employing the data points as vertices and adding edges, triangles and higher-dimension cells according to suitable rules. If K is a faithful topological representation of X, then we can obtain Betti numbers $\beta_k = \beta_k(X)$ by computing the Betti numbers $\beta_k(K)$ of K [21]. Various simplicial complexes can be built from X, as a Čech (VR) complex may be as large as an $(\mid S \mid -1)$-simplex. In practical computations, we usually use the witness complex [21].

For larger data sets, the subset $L \subset S$ is selected as the only vertex, which is known as a landmark point. One of the most common methods of choosing landmark points is to inductively select the landmarks, which is named sequential maxmin.

Table 1 The sizes of the largest subspaces of M_m with the topology of the Klein bottle

	M_3	M_5	M_7	M_9	M_{11}
The proportion of the largest subspace in M_m	29.4%	20.7%	15.5%	11.6%	7.8%

Given the landmarks L of a point set S, we set $m_p(s)$ as the distance from $s \in S$ to its $(p+1)$-th nearest landmark point. We define the witness complex $W(S, L, \epsilon)$ as follows: (a) L is the set of vertices; (b) for $p > 0$, the p-simplex $[l_0 l_1 ... l_p]$ belongs to $W(S, L, \epsilon)$ when all faces of $[l_0 l_1 ... l_p]$ belong to $W(S, L, \epsilon)$ and if a witness $s \in S$ that satisfies

$$\max\{d(l_0, s), d(l_1, s), ..., d(l_p, s)\} \leq \epsilon + m_p(s) \text{ exists.}$$

A lazy witness complex may be similarly defined as a witness complex. For additional details of lazy witness complexes and examples, please refer to [3, 21].

A parameter ϵ is needed when building a global complex from a point set. The ϵ cannot be too small or too large, and there is no best value of ϵ that first-rate catches the topology of the set. For example, 20 points and 4 lazy witness complexes are shown in Fig. 1, where we consider 5 landmark points, v=1, and ϵ=0.6, 0.9, 3, and 3.5. The point set is nearly obtained from a circle, and the Betti numbers of a circle are Betti_0 =Betti_1= 1. Can this result be concluded? We discover that the sequence of lazy witness complexes increases from (a) to (d). No hole exists in Fig. 1a and b, and a new hole appears in Fig. 1c. With an increase in ϵ, the hole vanishes, and it is fully filled in Fig. 1d. The image has one hole; hence, Fig. 1c gives the correct answer.

If previous information about the image is not available, we cannot conclude which ϵ is correct, and no optimal value of ϵ is obtained. We need a method for asserting which holes are indispensable and which holes can be safely neglected. The normal topological structures of homotopy and homology do not provide any identification [10]. Persistence was established in [8] and refined in [20]; it is a rigorous response to this problem.

3 Persistent homology

When we only have the finite sampled points from an underlying space X, and without a previous message of X, it is very difficult to estimate a value of ϵ that creates a simplicial complex whose homology group is isomorphic to that of X. To solve the problem, the authors of [8] introduce persistence. Assuming $\epsilon \leq \widetilde{\epsilon}$, a natural inclusion mapping exists: $LW_v(S, L, \epsilon) \hookrightarrow LW_v(S, L, \widetilde{\epsilon})$. Due to the functoriality, the linear transformation $H_k(LW_v(S, L, \epsilon)) \mapsto H_k(LW_v(S, L, \widetilde{\epsilon}))$ exists for each $k \geq 0$, where $H_k(LW_v(S, L, \epsilon))$ is the k th homology group of $LW_v(S, L, \epsilon)$. Edelsbrunner et al. [8] observed that the directed system of vector spaces $H_k(LW_v(S, L, \epsilon))$ should be investigated, including all previously mentioned linear transformations for analyzing the homology of the underlying space using points sampled from it. Barcodes (that consist of finite intervals) and isomorphic classes of directed systems of vector spaces are demonstrated to have a one-to-one correspondence [20]. The barcodes can be computed from sampled points by using the software package JAVAPLEX developed in [3].

Intuitively, the intervals of a barcode correspond to the lifetimes of the topological properties. A new topological feature emerges at the initial point of an interval and disappears at the final point of the interval.

Recall that the i-th Betti number β_i=rankH_i is approximately the count of i-dimensional holes in a complex H_i, and β_i can be calculated by the barcodes. An interval $[\epsilon_0, \epsilon_1]$ of a barcode means that a hole of the complex arises at $\epsilon = \epsilon_0$ and disappears at $\epsilon = \epsilon_1$.

Long intervals can be intuitively explained to correspond to practical topological properties of the space, while tiny intervals are derived from irregularities in the point sampling. Figure 2 displays a barcode plot of the homology of the sampled points in Fig. 1. For the

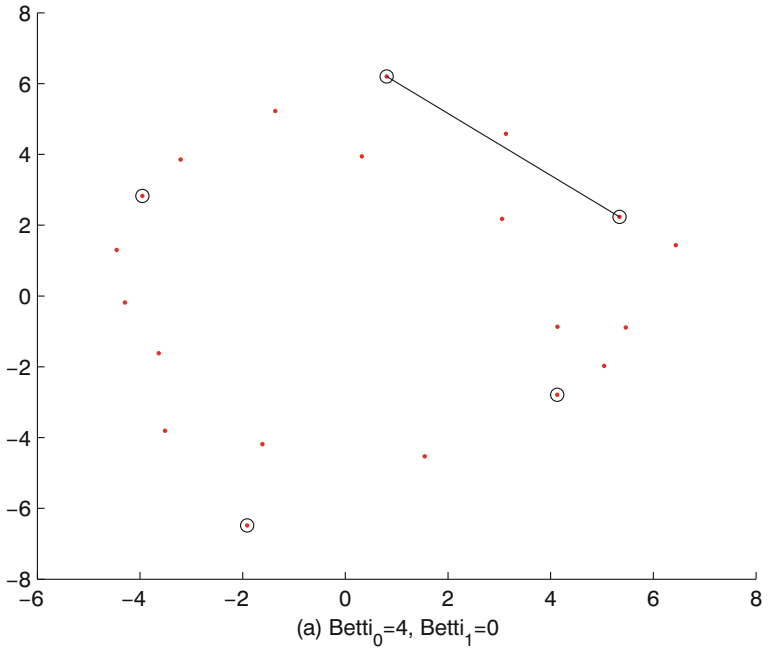

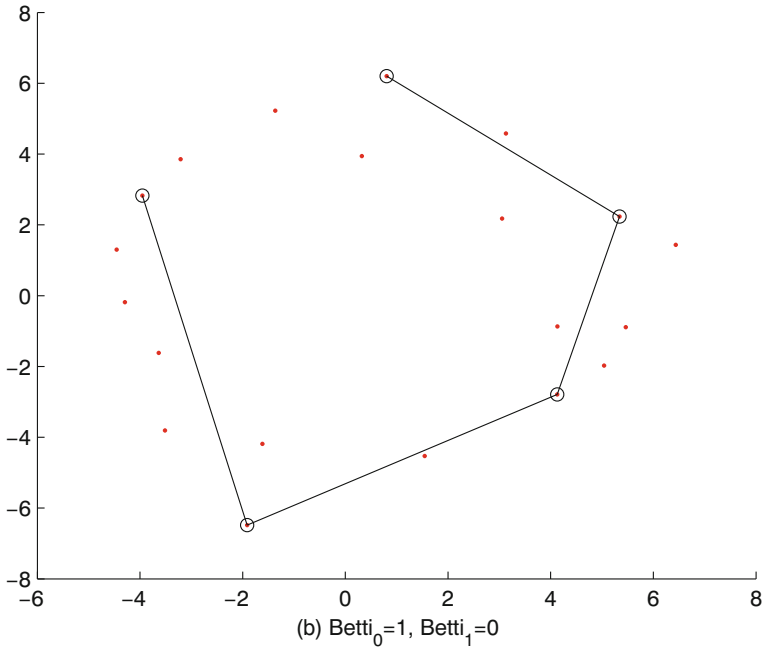

Fig. 1 Four lazy witness complexes for 20 points sampled nearly from a circle. As ϵ is increased, a hole appears and disappearss

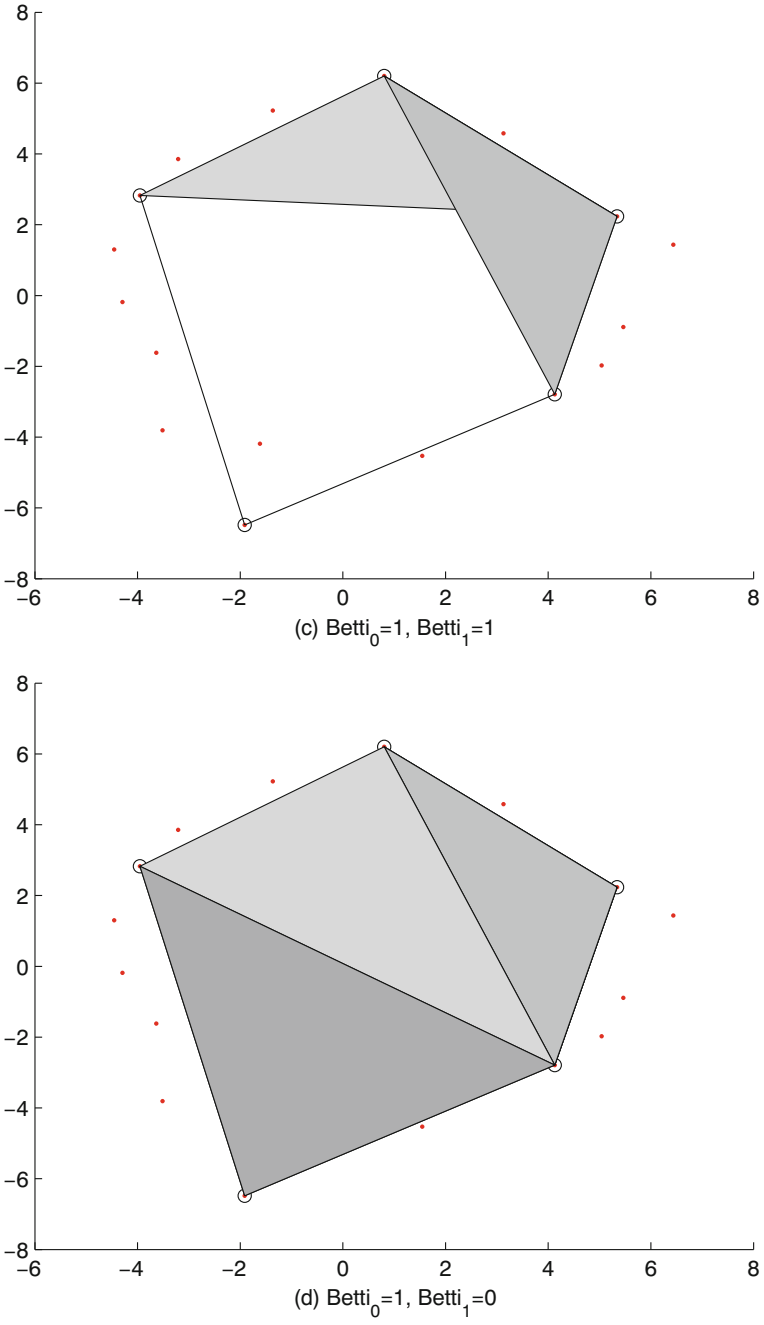

Fig. 1 (continued)

case $\epsilon = 3$, the barcodes yield $\beta_0 = 1$, $\beta_1 = 1$ and $\beta_2 = 0$, which are Betti numbers of the lazy witness complex in Fig. 1c. Figure 2 shows the topological property of a circle.

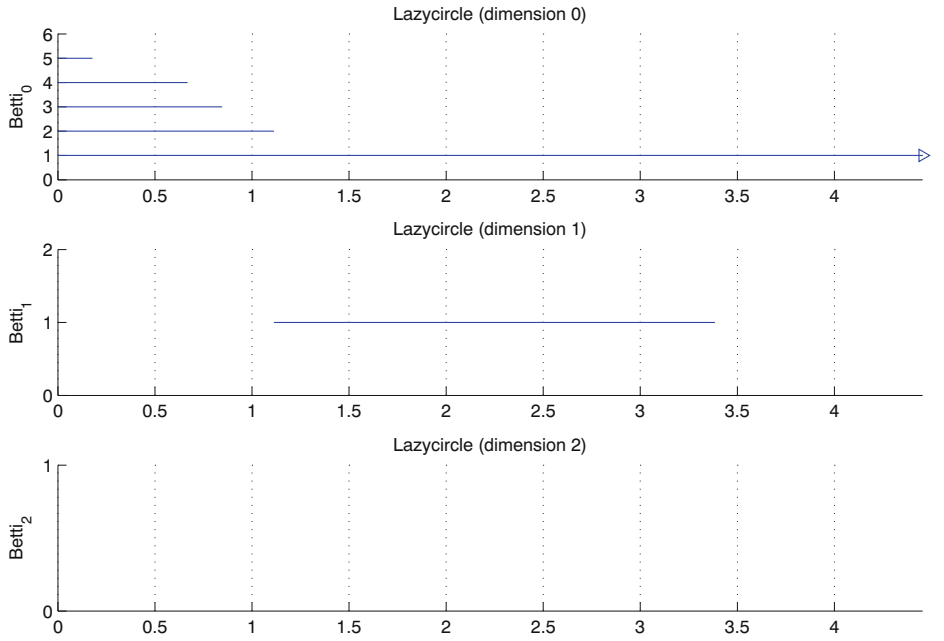

Fig. 2 The barcodes for the sequence of lazy witness complexes $LW_1(S, L, \epsilon)$, $0 \leq \epsilon \leq 4.45$, built in Fig. 1

4 The spaces of range image patches

We extract high-contrast 3×3, 5×5, 7×7, 9×9, and 11×11 patches from the range images. The data sets are extracted from the Brown database of approximately 200 range images [12]; refer to Fig. 3 for samples.

The main space M_m (for m= 3, 5, 7, 9, 11) in this paper consists of $m \times m$ patches of high contrast that are acquired in 6 steps, which are similar to the procedures in [2, 6, 15]. Thus, we obtain a set of approximately 400000 high-contrast $m \times m$ patches (unit vectors); it is our main space M_m for $m = 3, 5, 7$. The main spaces M_9 and M_{11} contain approximately 280000 high-contrast 9×9 patches and 190000 high-contrast 11×11 patches, respectively. For computational feasibility, we randomly select 50000 patches from each M_m; these spaces are denoted by $\widetilde{M}_3$, $\widetilde{M}_5$, $\widetilde{M}_7$, $\widetilde{M}_9$ and $\widetilde{M}_{11}$.

We describe an outline of the proposed methodology as in Fig. 4.

5 Results for $\widetilde{M}_3$, $\widetilde{M}_5$, $\widetilde{M}_7$, $\widetilde{M}_9$ and $\widetilde{M}_{11}$

We research the topological features of noisy point-cloud datasets $\widetilde{M}_3$, $\widetilde{M}_5$, $\widetilde{M}_7$, $\widetilde{M}_9$ and $\widetilde{M}_{11}$ using the persistent homology method. We aim to identify that $\widetilde{M}_3$, $\widetilde{M}_9$ and $\widetilde{M}_{11}$ have a circular behavior. The results in [2] suggest the existence of core subsets in $\widetilde{M}_5$ and $\widetilde{M}_7$, which have the topology of a circle.

To discover the circle, we first identify the core subsets. The concept of local density for a space X is defined in [2, 6]; let $\rho_j(x) = \mid x - x_j \mid$, where $j > 0$ and x_j are the j-th closest neighbors of $x \in X$. The size of j describes the local density at x, in which a larger

Fig. 3 Samples from the Brown range image database by Huang and Lee

value of j provides a more global density approximation, while a small value of j gives a local approximation. For a given j, all elements of X are arranged in descending order of density, and the elements of X with the top $w\%$ density are chosen (denoted $X(j, w)$) for topological computations. In many cases, the core subsets $X(j, w)$ of X may offer important topological properties, which are probably lost for the whole X.

We study the core subsets $M^m(j, w)$ of $\widetilde{M}_m$ when $m = 3, 5, 7, 9, 11$. $M^m(j, w)$ is a two-parameter subset that, for the right values of j and w, represents a suitable core.

Lee et al. [15] discover that 3×3 high-contrast range patches are intensively gathered near the binary patches. Perhaps because few (only 510) 3×3 binary patches exist, as noted in [2], the core subset $M^3(300, 30)$ does not show a clear topological property. Considering

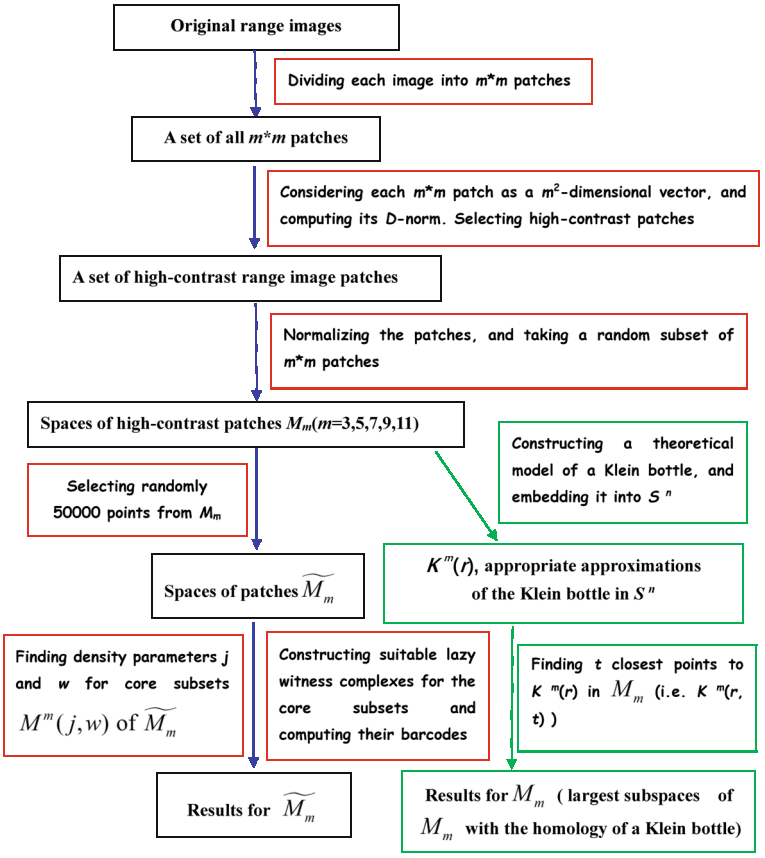

Fig. 4 An outline of the method used in the paper

the density parameter $j = 900$ and cut percentage $w = 30$, one sample plot result of the core subset $M^3(900, 30)$ is given in Fig. 5 as evidence of circular topology. The plot of $M^3(900, 30)$ displays one long line in the 0-dimensional $Betti_0$ and one long $Betti_1$ line, which correspond to a circle, as shown in Fig. 6. We construct the discrete cosine transform for $m \times m$ patches of $M^m(j, w)$ with DCT basis vectors.

We project core subsets onto two of the DCT basis vectors, which are vertical and horizontal linear gradients; the results are shown in Figs. 6, 7, 8, 9, and 10, where a circle is visible in them. Choosing 35 to 70 landmarks, we repeatedly perform experiments using $M^3(900, 30)$, $M^3(800, 30)$ and $M^3(700, 30)$; the experimental results are robust.

For 5×5 and 7×7 patches, we consider their core subsets $M^5(300, 30)$ and $M^7(300, 30)$. Figures 11 and 12 show the specimen PLEX plots for the core subsets. The two plots show that they have the topology of a primary circle, as indicated by Adams and Carlsson in [2].

For 9×9 and 11×11 patches, we consider their core subsets $M^9(200, 20)$ and $M^{11}(200, 20)$. Figures 13 and 14 are examples of their barcode plots, which exhibit the topology of a circle. By selecting different landmark points, we carry out many times experiments on $M^9(200, 20)$ and $M^{11}(200, 20)$ respectively, and show that the results are robust. In every experiment, the circular profile $\beta_0 = \beta_1 = 1$ is found for almost full range of ϵ

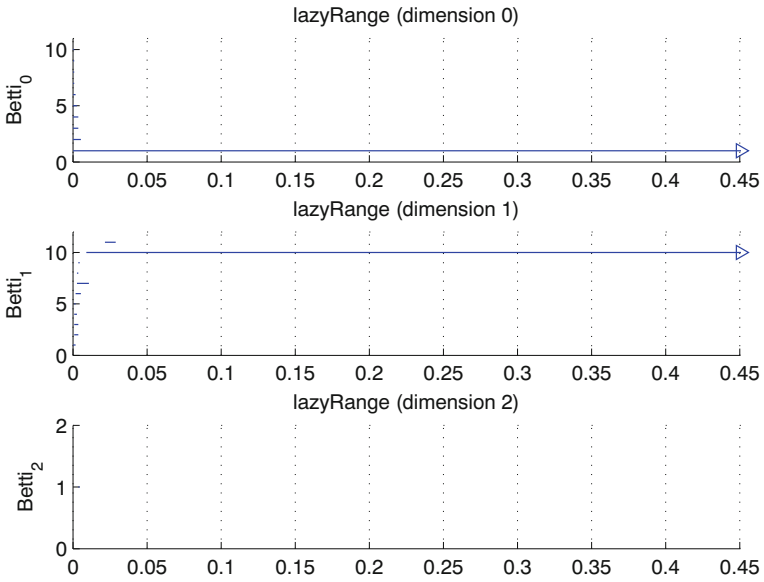

Fig. 5 Barcodes for $M^3(900, 30)$

values, and there is no other Betti interval or there are other very short Betti intervals (Figs. 5, 11, 12, 13, and 14).

In 2015, Adams et al. in [1] study 5×5 range patches and 3×3 optical flow patches, where the optical flow data set was created in [16] from the range images of the Brown database; the authors employ the nudged elastic band technique to show that 5×5 range

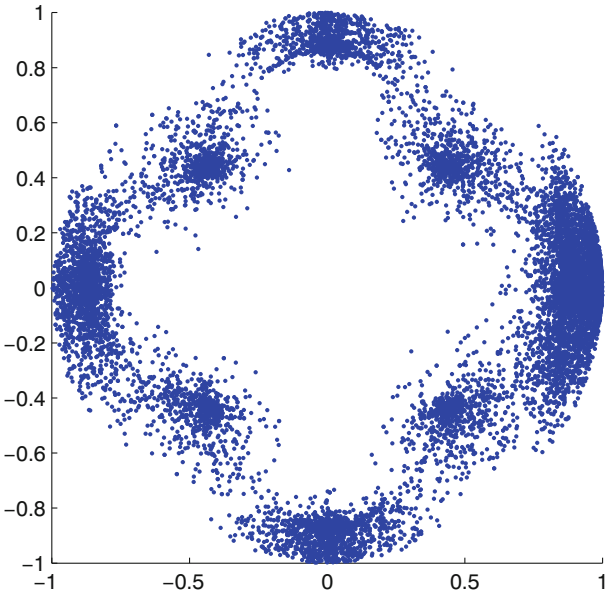

Fig. 6 Projection of $M^3(900, 30)$ onto linear gradients

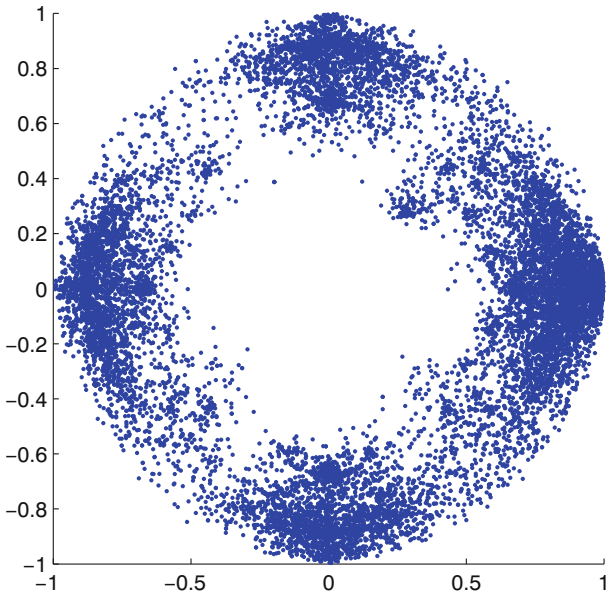

Fig. 7 Projection of $M^5(300, 30)$ onto linear gradients

patches and 3×3 optical flow patches exhibit circular behavior. The results of this paper and [1] demonstrate that 3×3 range patches have a topological property that is similar to that of 3×3 optical flow patches.

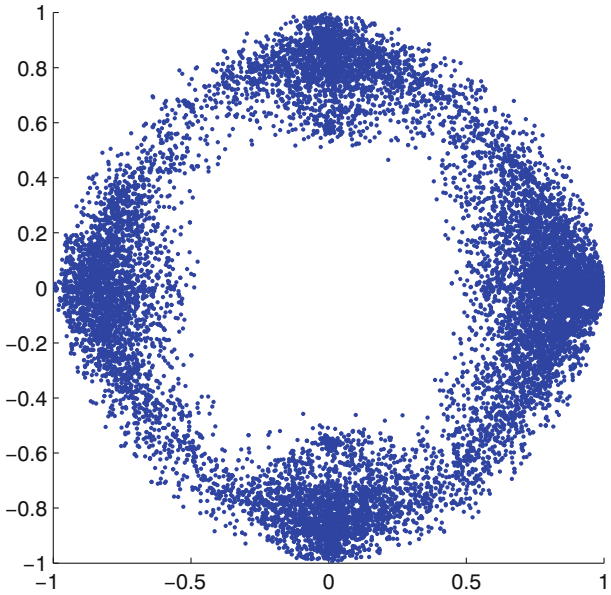

Fig. 8 Projection of $M^7(300, 30)$ onto linear gradients

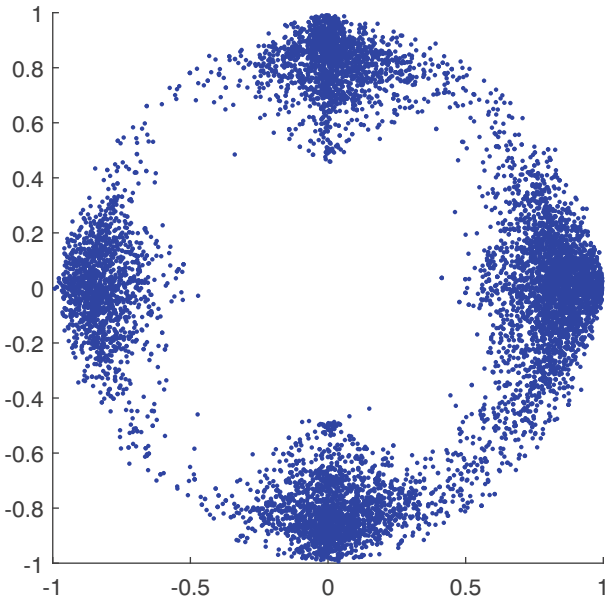

Fig. 9 Projection of $M^9(200, 20)$ onto linear gradients.

Remark 1 Recently, the authors of [7] have shown that 3×3 range image patches have a core set with topology of a circle by using the nudged elastic band method; the core set in [7] is different from our set $M^3(900, 30)$. The circular behavior of 9×9 range image patches is shown in [19]; the 9×9 patch set of [19] is different from our M_9.

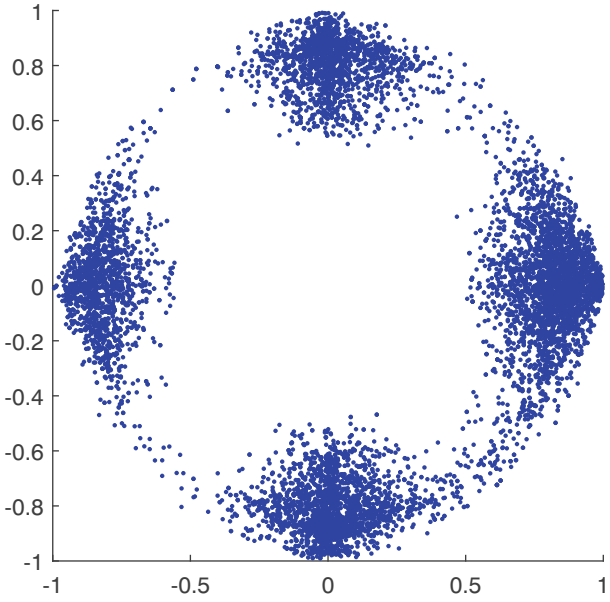

Fig. 10 Projection of $M^{11}(200, 20)$ onto linear gradients

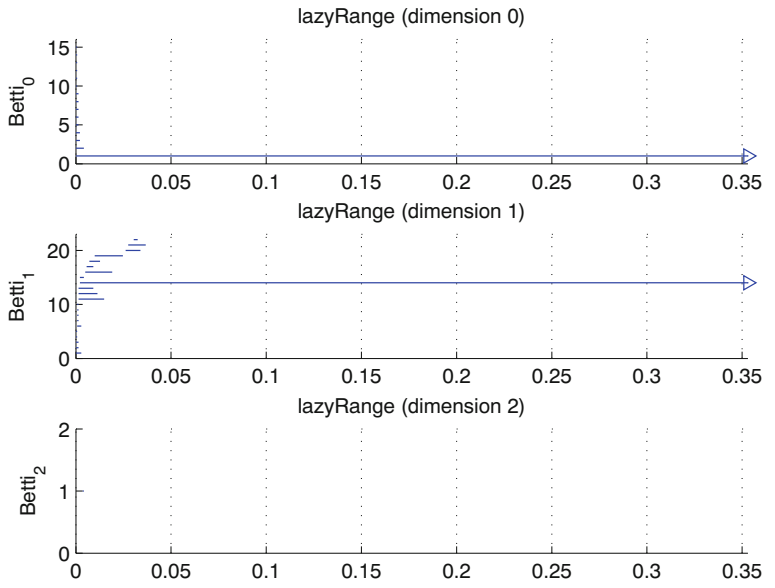

Fig. 11 Barcodes for $M^5(300, 30)$

In [6], the core subset of optical patches, with values of $j = 15$ and $w = 30$, was observed to have the first Betti number $\beta_1 = 5$. By computing the Betti number β_0, the results indicate [6] that a main circle and two secondary circles arise in the lower density. A decrease in the density parameter j-values causes a more localized density sensitivity. In [6], the space $X(j, w)$ of optical patches was shown to span a two-manifold: the Klein bottle

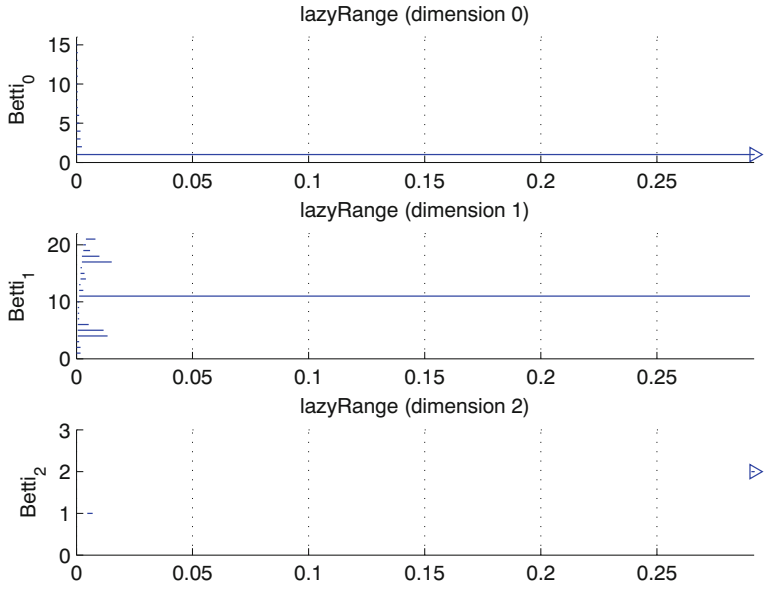

Fig. 12 Barcodes for $M^7(300, 30)$

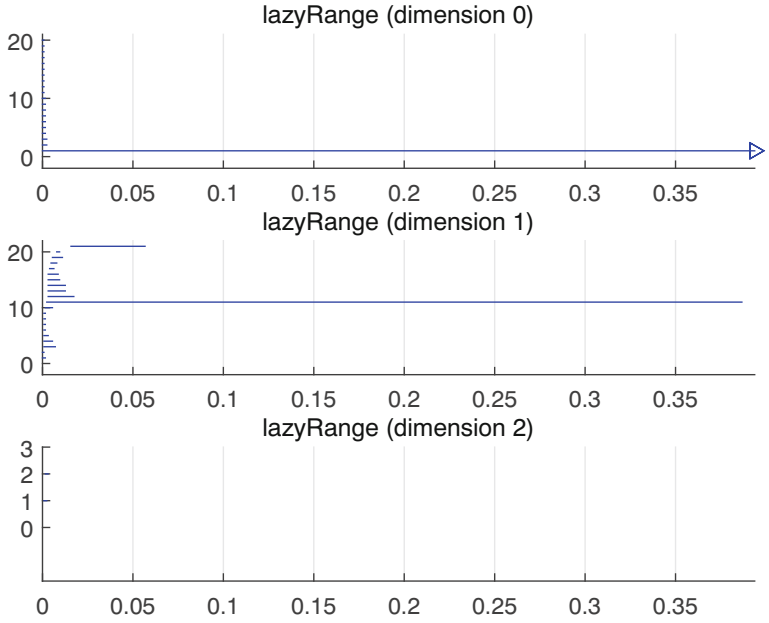

Fig. 13 Barcodes for $M^9(200, 20)$

for some appropriate values of the cut parameter w and the density parameter j. Additional topological features of spaces of range patches are not easily detected using core subsets with lower values of j and w, as previously demonstrated for optical patches. We conducted

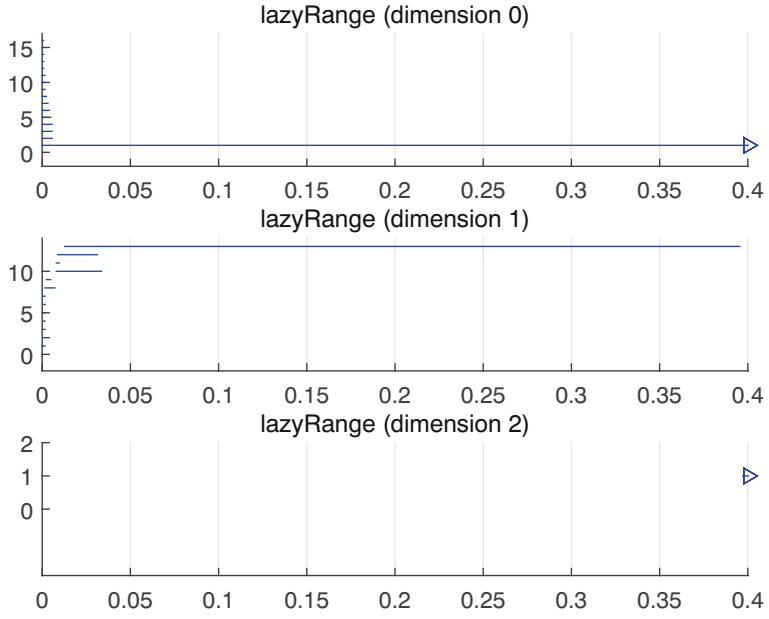

Fig. 14 Barcodes for $M^{11}(200, 20)$

five hundred trials using $M^m(j, w)$ and selected different landmark points and lower values of j and w. We cannot obtain desirable results. Figure 15 shows the experimental results for $M^3(200, 20)$; $M^3(200, 20)$ has Betti number $\beta_0 = 1$, and $\beta_1 = 5$ in a small range of ϵ values, but the experimental result is very unstable. We cannot conclude a definitive result for $M^3(200, 20)$. In sections 6 and 7, we further analyze the topological features of spaces of range patches using techniques of Carlsson et al. [6].

6 Klein bottle and spaces of polynomials with two variables

The authors of [6] show the existence of a space of optical patches, whose first Betti number is 5. The space is reasonably depicted as a three-circle model (Fig. 16), which is represented by C_3. C_3 consists of a primary circle (S_{lin}) and two secondary circles (labeled S_v and S_h). S_v and S_h intersect S_{lin} at two points and do not cross each other.

Recall that the standard expression of a Klein bottle can be described as a quotient space of a planar square (Fig. 17) [11]. The 3-circle model C_3 may be sensibly embedded in a Klein bottle, as shown in Fig. 17. The level black lines constitute the primary circle S_{lin}. The vertical red and blue lines constitute the secondary circles that are separately relevant to S_v and S_h, as shown in Fig. 17.

In section 4, each $m \times m$ patch of range images was processed as a unit vector in $\mathbb{R}^{m\times m}$ (m=3, 5, 7, 9, 11). To determine the topological properties of various subspaces of M_m (m=3, 5, 7, 9, 11), we establish a relation between the $m \times m$ patches and the 2-degree polynomials with double-variable polynomials P, which have the form $u_3(u_1x + u_2y)^2 + u_4(u_1x + u_2y)$, where u_1, u_2, u_3, u_4 are real parameters such that (u_1, u_2) and (u_3, u_4) belong to the planar unit circle S^1. For additional details, please refer to [5].

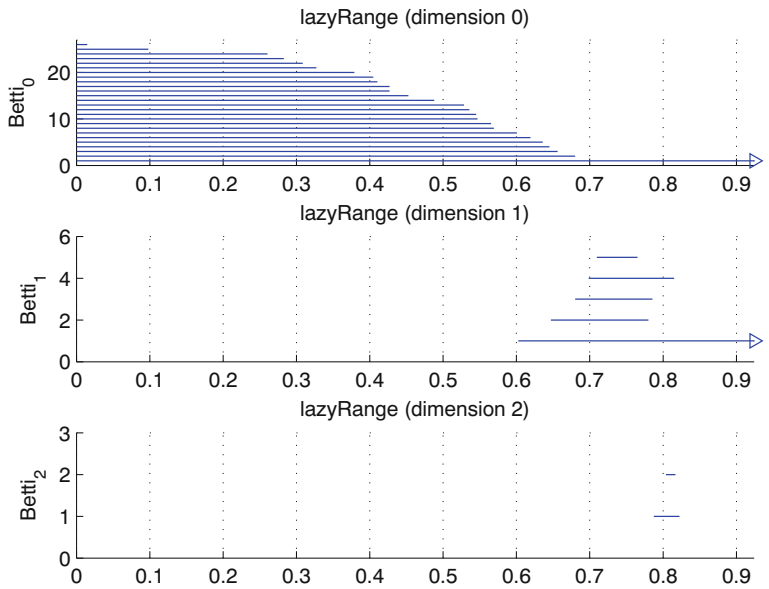

Fig. 15 Barcodes for $M^3(200, 20)$

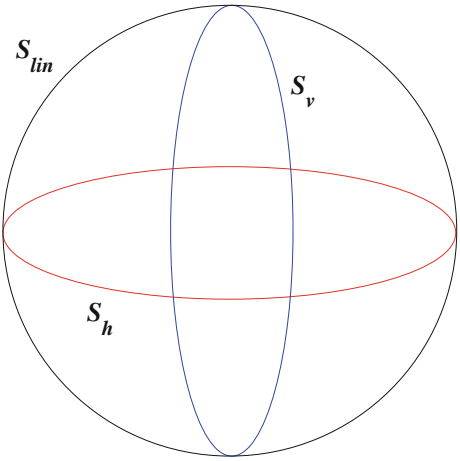

Fig. 16 Three-circle model

We introduce the mapping $f : S^1 \times S^1 \longmapsto P$ by $(u_1, u_2, u_3, u_4) \longmapsto u_3(u_1x + u_2y)^2 + u_4(u_1x + u_2y)$ [6]. We note that the mapping f is onto P but is not a one-to-one correspondence. Thus, we obtain the relation

$$(u_1, u_2, u_3, u_4) \sim (-u_1, -u_2, u_3, -u_4).$$

If we use $(\cos\omega_1, \sin\omega_1, \cos\omega_2, \sin\omega_2)$ instead of (u_1, u_2, u_3, u_4), $\omega_1 \in [0, 2\pi]$ and $\omega_2 \in [0, 2\pi]$, then the relationship can be stated by $(\omega_1, \omega_2) \sim (\pi + \omega_1, 2\pi - \omega_2)$. Hence, P is homeomorphic to $S^1 \times S^1/((\omega_1, \omega_2) \sim (\pi + \omega_1, 2\pi - \omega_2))$.

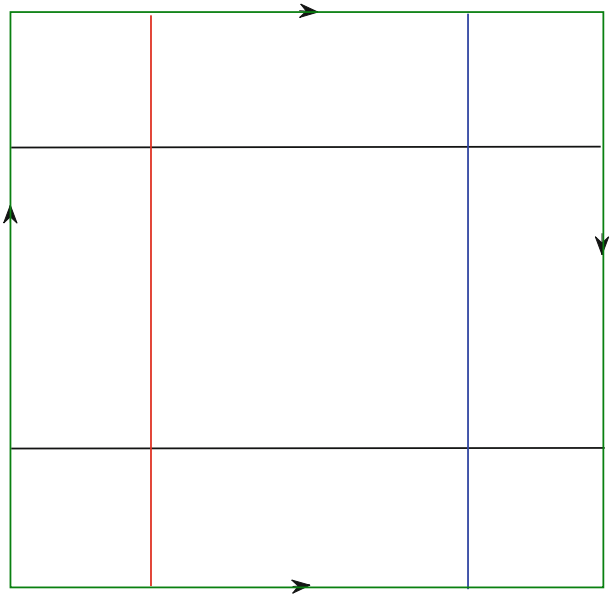

Fig. 17 A representation of a Klein bottle by pasting a square

A similar method exists to form a torus as a formation of the Klein bottle. The result of the mapping f that acts on the torus is demonstrated in Fig. 18. The right half is mapped onto the left half by f, according to the identifications on the boundaries as illustrated by the arrows. Each half of the figure is a denotation of a Klein bottle. Thus, the im$f$ is homeomorphic to a Klein bottle, and P is homeomorphic to the Klein bottle ([6]).

We note that the three-circle space C_3 is also involved in the space P. For set $(u_3, u_4) = (0, 1)$ and $(u_1, u_2) \in S^1$, we obtain the primary circle of C_3 and secondary circles when we let $u_1 = 1, u_2 = 0$ and $u_1 = 0, u_2 = 1$.

We define the mapping $h_3 : P \longmapsto S^8$ as a composite for computing the values of the polynomials at the planar grid points $H_3 = \{-1, 0, 1\} \times \{-1, 0, 1\}$ by removing the mean and similarly normalizing $h_5 : P \longmapsto S^{24}$ at $H_5 = \{-2, -1, 0, 1, 2\} \times \{-2, -1, 0, 1, 2\}$, $h_7 : P \longmapsto S^{48}$ at $H_7 = \{-3, -2, -1, 0, 1, 2, 3\} \times \{-3, -2, -1, 0, 1, 2, 3\}$, $h_9 : P \longmapsto S^{80}$ at H_9={-4, -3, -2, -1, 0, 1, 2, 3, 4}× {-4, -3, -2, -1, 0, 1, 2, 3, 4}, and $h_{11} : P \longmapsto S^{120}$ at H_{11}={-5, -4, -3, -2, -1, 0, 1, 2, 3, 4, 5}× {-5, -4, -3, -2, -1, 0, 1, 2, 3, 4, 5}.

Proposition 1 *Every mapping h_m(m=3, 5, 7, 9, 11) is one-to-one.*

The proof is nearly identical to that of [6].

A one-to-one continuous mapping from a compact space to its image is a homeomorphic mapping; hence, by the Proposition, each image of $h_m (m = 3, 5, 7, 9, 11)$ is homeomorphic to a Klein bottle.

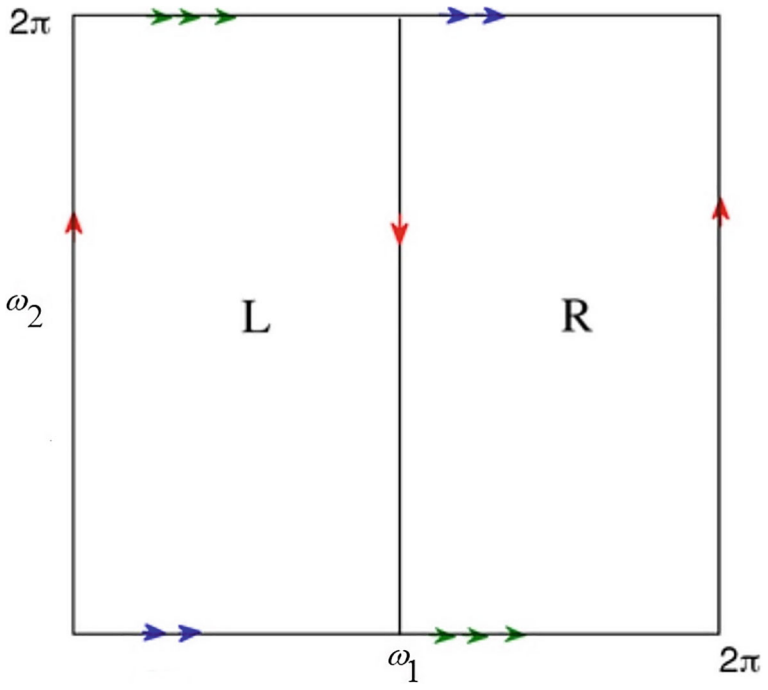

Fig. 18 The image of the mapping f, a representation of a Klein bottle [6]

7 Embedding of a Klein bottle into S^8, S^{24}, S^{48}, S^{80} and S^{120}

In the previous section, we conclude that each of S^8, S^{24}, S^{48}, S^{80} and S^{120} has a subspace with the topology of a Klein bottle. We have mapped our spaces M_m (m=3, 5, 7, 9, 11) into spheres S^8, S^{24}, S^{48}, S^{80} and S^{120}, respectively, as discussed in section 4. To determine the topological properties of various core subsets of M_m, we embed the Klein bottle into the spheres, where M_3, M_5, M_7, M_9 and M_{11} exist. In this section, we provide experimental results that support our theoretical conclusion of the previous section.

For embedding the space C_3 into a unit ball, we initially and randomly elect 300 points $\{(a_1, b_1), ..., (a_{300}, b_{300})\}$ from S^1. We evaluate $h_m \circ f$ images of the 300 points for $u_3 = 0, u_4 = 1$; $u_1 = 1, u_2 = 0$; and $u_1 = 0, u_2 = 1$. The set of all images is denoted as $C^m(300)$, $m = 3, 5, 7, 9, 11$. We know that $C^3(300)$, $C^5(300)$, $C^7(300)$, $C^9(300)$ and $C^{11}(300)$ are sampled from the images of C_3 with the maps $h_3 \circ f$, $h_5 \circ f$, $h_7 \circ f$, $h_9 \circ f$ and $h_{11} \circ f$, respectively. Figure 19 displays one sample barcode plot of $C^3(300)$, which demonstrates that $C^3(300)$ has Betti numbers $\beta_0 = 1$, $\beta_1 = 5$ and $\beta_2 = 0$, that is, $C^3(300)$ is an appropriate approach of the image of C_3 using the map $h_3 \circ f$. We obtain similar results for $C^5(300)$, $C^7(300)$, $C^9(300)$ and $C^{11}(300)$, as separately shown in Figs. 20, 21, 22 and 23. After conducting many experiments, we discover that the results are extremely steady.

To embed a Klein bottle into a unit ball, first, we uniformly select r points from the unit circle (denoted by $\{x_1, ..., x_r\}$). All possible tuples (x_i, x_j) compose a set of the torus $S^1 \times S^1$. Second, we map each of the r^2 points into S^8, S^{24}, S^{48}, S^{80} and S^{120} by maps $h_3 \circ f$, $h_5 \circ f$, $h_7 \circ f$, $h_9 \circ f$ and $h_{11} \circ f$ and separately denote the set of images of each map as $K^3(r)$, $K^5(r)$, $K^7(r)$, $K^9(r)$ and $K^{11}(r)$. The points are sampled from the images of the Klein bottle with the maps $h_3 \circ f$, $h_5 \circ f$ and $h_9 \circ f$ and $h_{11} \circ f$. We consider r=160 for m=3, 5, 7, and r=200 for m=9, 11. One sample barcode plot of the space $K^3(160)$ is displayed in Fig. 24, which yields the Betti numbers of a Klein bottle (with the mod 2):

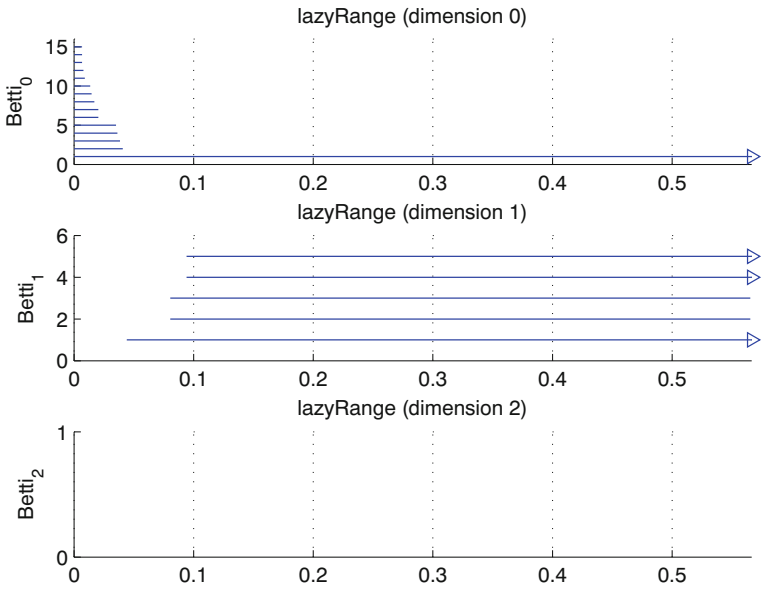

Fig. 19 Barcodes for $C^3(300)$

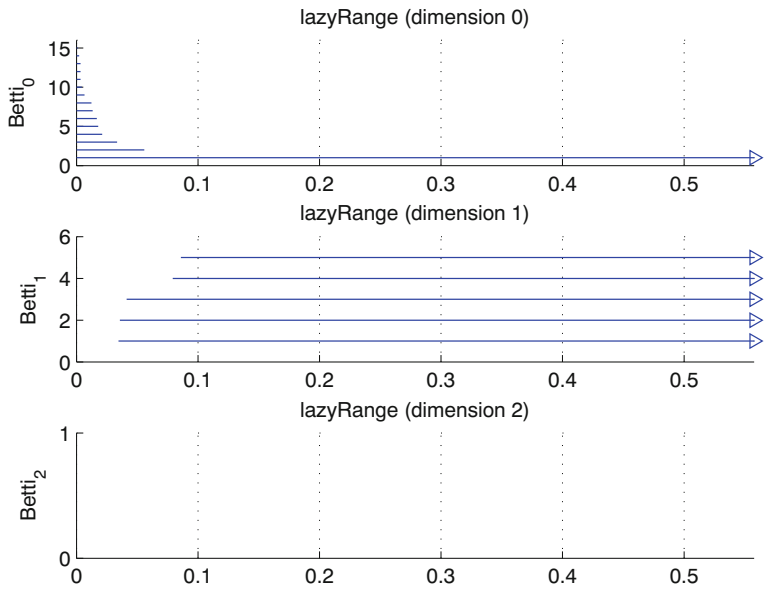

Fig. 20 Barcodes for $C^5(300)$

$\beta_0 = 1, \beta_1 = 2$ and $\beta_2 = 1$. Thus, $K^3(160)$ is an acceptable estimation of the Klein bottle in S^8. For different landmark points (from 30 to 80) and different max-filtration values, the result is very stable. We have similar results for $K^5(160)$, $K^7(160)$, $K^9(200)$ and $K^{11}(200)$, as shown in Figs. 25, 26, 27 and 28, respectively.

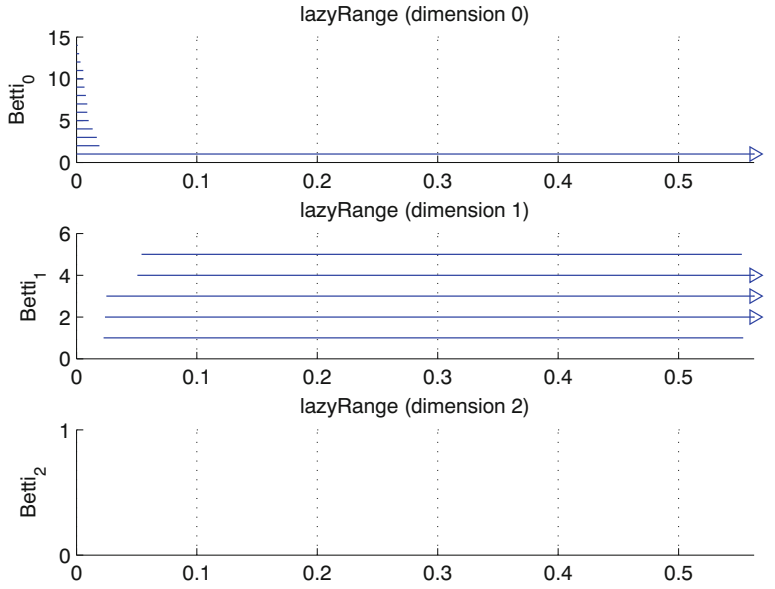

Fig. 21 Barcodes for $C^7(300)$

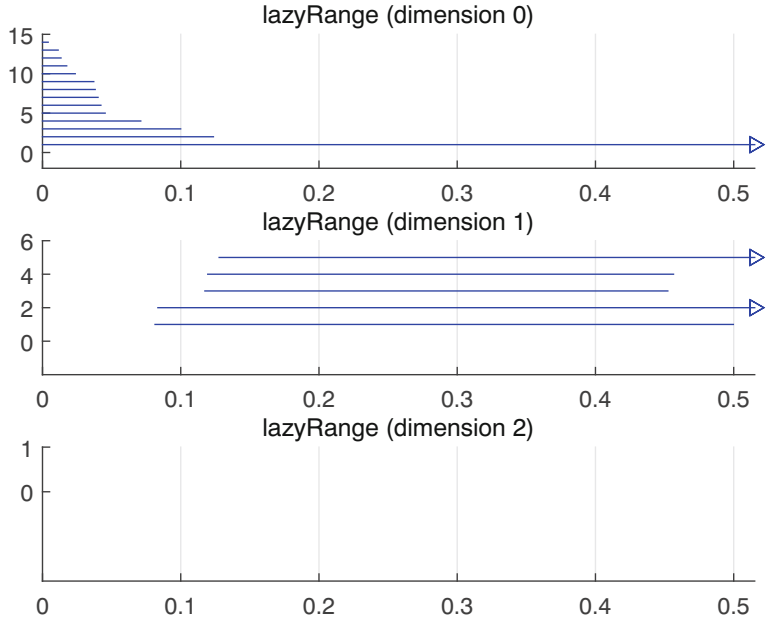

Fig. 22 Barcodes for $C^9(300)$

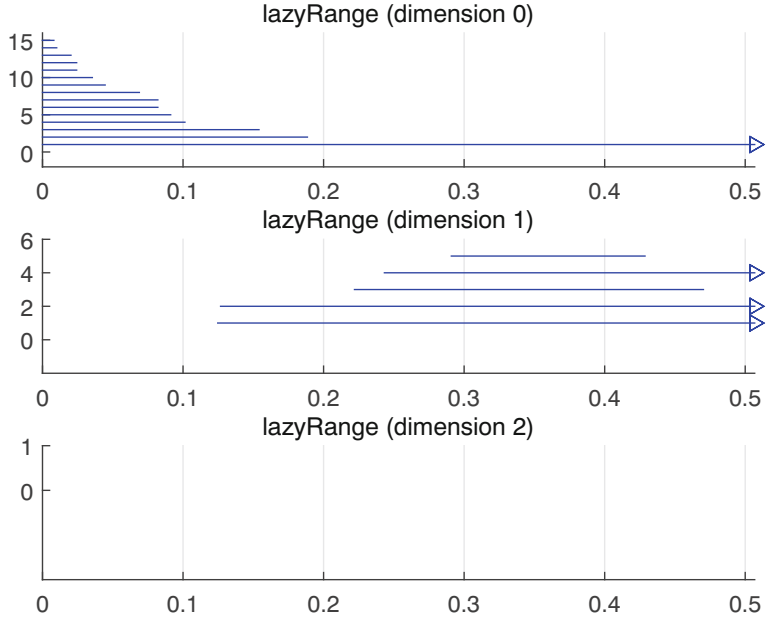

Fig. 23 Barcodes for $C^{11}(300)$

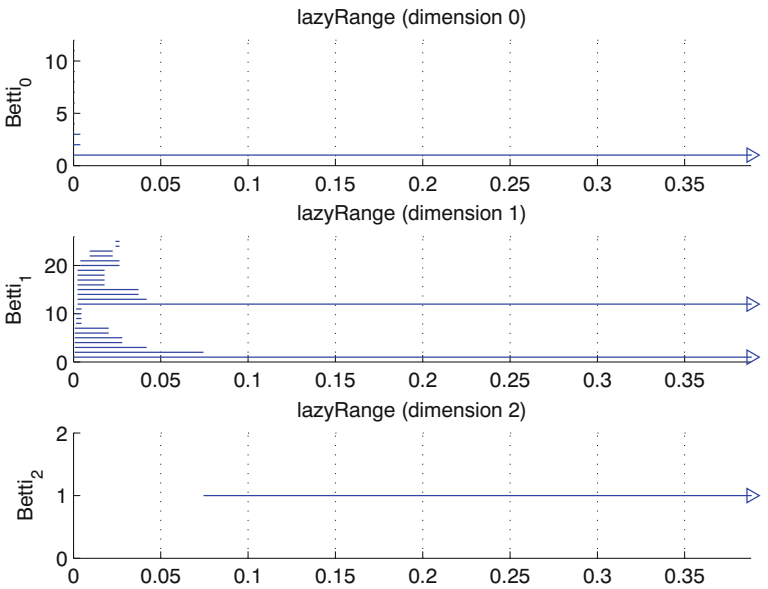

Fig. 24 Barcodes for $K^3(160)$

8 Results for M_3, M_5, M_7, M_9 and M_{11}

For optical patches, with a decrease in the density estimator j, the topology of the core sets $X(j, w)$ varies from the topology of a circle to that of the 3-circle space and then to

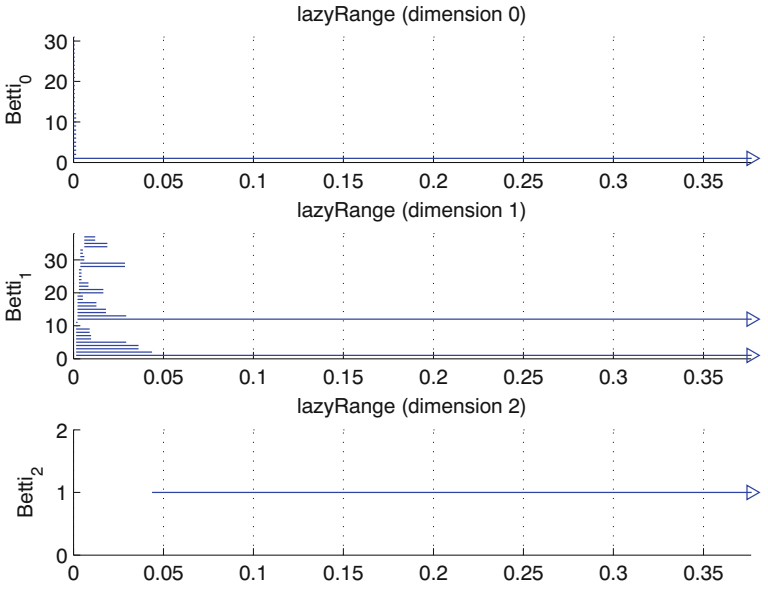

Fig. 25 Barcodes for $K^5(160)$

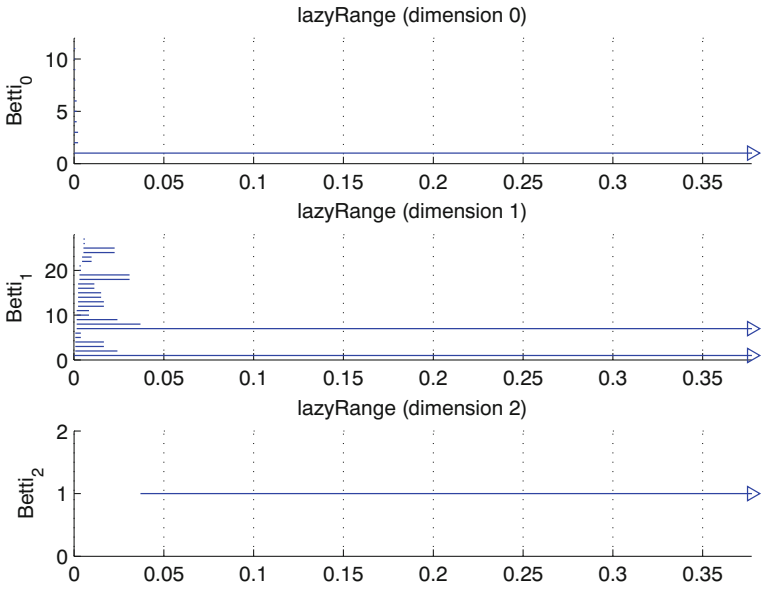

Fig. 26 Barcodes for $K^7(160)$

the Klein bottle [6]. For range patches, we do not obtain results that are similar to those of optical patches by the same way. For example, the core set $X(j, w)$ of M_3 is not obtained by employing appropriate parameter values of j and w, whose topology is identical to that of

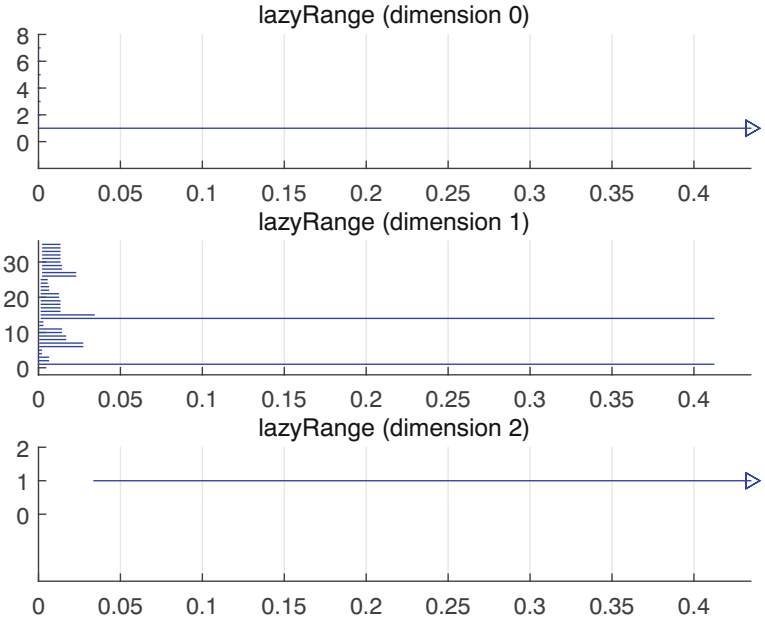

Fig. 27 Barcodes for $K^9(200)$

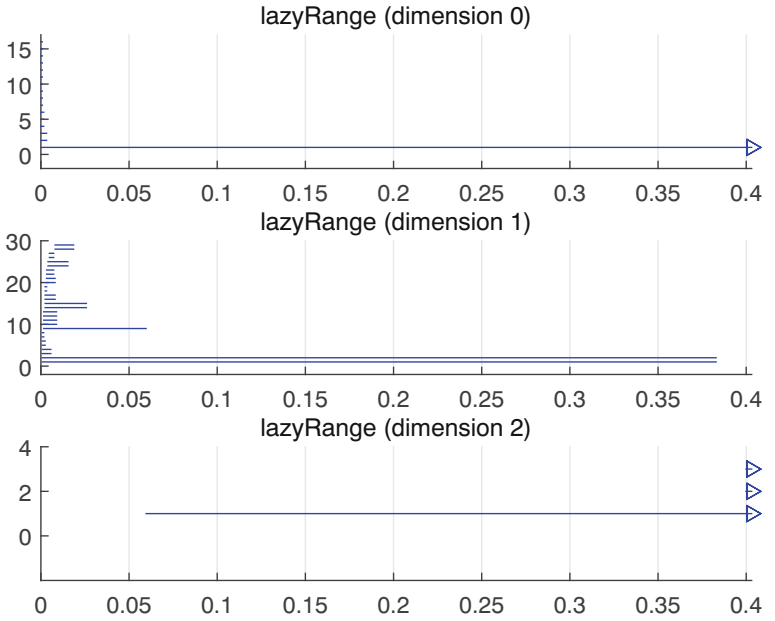

Fig. 28 Barcodes for $K^{11}(200)$

the Klein bottle. In this section, we will use an alternative approach to show that M_m (m=3, 5, 7, 9, 11) has a proper subset with the topology of C_3 and an appropriate subset with the topology of the Klein bottle.

For each $p \in C^3(300)$, we compute the Euclidean distance from p to all points of M_3 and identify the closest point of M_3, for which this distance is the smallest. Thus, we obtain a subspace of M_3 by gathering the closest points to each point $p \in C^3(300)$, and denote it by $CC^3(300)$. Using a similar approach, we obtain the subspaces $CC^m(300)$ of M_m for m =5, 7, 9, and 11.

One plot result of the space $CC^3(300)$ is shown in Fig. 29, which yields the Betti numbers $\beta_0 = 1$ from $\epsilon = 0.03$ to $\epsilon = 0.6$ and the $\beta_1 = 5$ from $\epsilon = 0.11$ to $\epsilon = 0.56$. Thus, $CC^3(300)$ has the topology of the three-circle space C_3. Figures 30, 31, 32 and 33 show that $CC^5(300)$, $CC^7(300)$, $CC^9(300)$ and $CC^{11}(300)$ have the topology of C_3. We conducted more than 100 trials on each of $CC^3(300)$, $CC^5(300)$, $CC^7(300)$, $CC^9(300)$ and $CC^{11}(300)$ by selecting different landmark points. The results are extremely robust.

As discussed in the previous section, each of S^8, S^{24}, S^{48}, S^{80} and S^{120} has the subspace $K^3(160)$, $K^5(160)$, $K^7(160)$, $K^9(200)$ and $K^{11}(200)$, respectively, and their topology is identical to that of the Klein bottle. We will describe how to experimentally identify subspaces of M_m (m=3, 5, 7, 9, 11) with the topology of a Klein bottle. Considering M_3 as an example, the procedure is described as follows:

For any p of $K^3(160)$, we compute the Euclidean distance from p to all points of M_3. Thus, we obtain a subspace of M_3 by considering all t closest points to $p \in K^3(160)$ and denote it by $K^3(160, t)$. Using a similar method, we obtain the subspaces $K^5(160, t)$, $K^7(160, t)$, $K^9(200, t)$, and $K^{11}(200, t)$ of M_5, M_7, M_9 and M_{11}, respectively.

One sample barcode result for the space $K^3(160, 3)$ is shown in Fig. 34, which yields the Betti numbers $\beta_0 = 1$, $\beta_1 = 2$, and $\beta_2 = 1$ for ϵ values from 0.14 to 0.31. This result

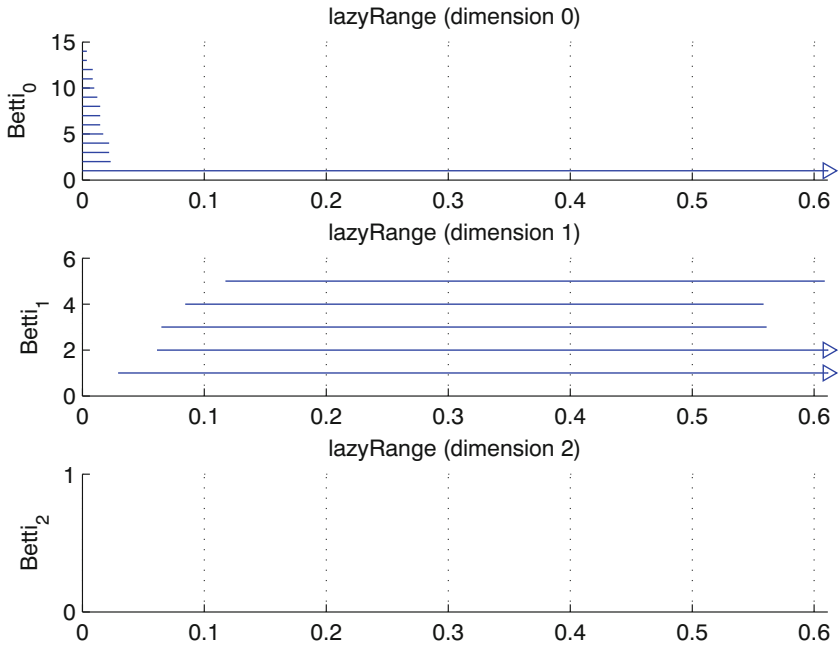

Fig. 29 PLEX results for $CC^3(300)$

indicates that $K^3(160, 3)$ has the topology of a Klein bottle. Figures 35, 36, 37 and 38 show that $K^5(160, 9)$, $K^7(160, 9)$, $K^9(200, 7)$ and $K^{11}(200, 7)$ have the topology of a Klein bottle. We perform more than 200 experiments for $K^3(160, t)$ at $t = 1, 2, 3, 5$; hence,

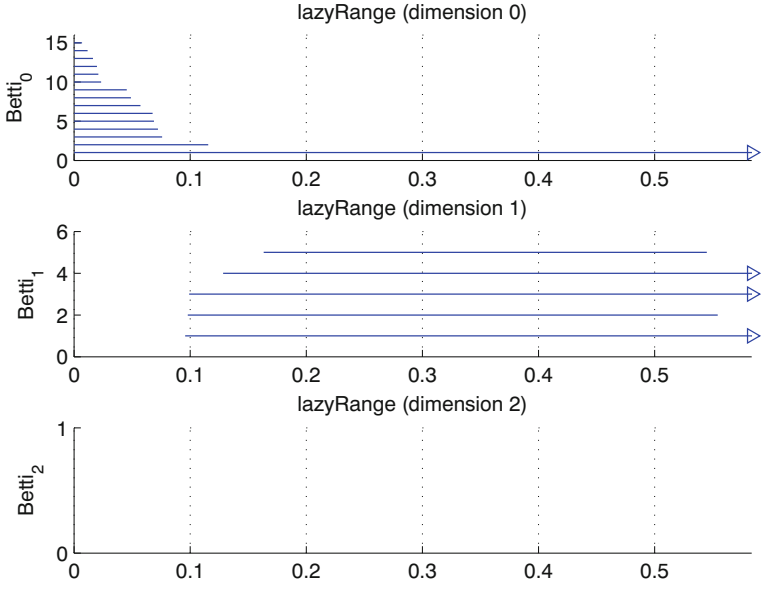

Fig. 30 PLEX results for $CC^5(300)$

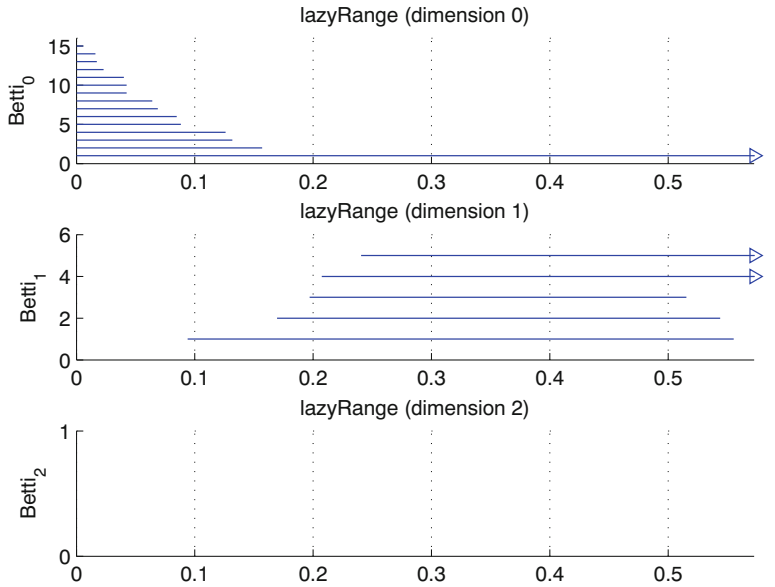

Fig. 31 PLEX results for $CC^7(300)$

the result is very steady. The results of $K^5(160, t)$ $(t = 3, 5, 7, 9)$ and $K^7(160, t)$ $(t = 5, 7, 9)$ are also very steady. However, the results for $K^9(200, 7)$ and $K^{11}(200, 7)$ (including $K^9(200, t)$ and $K^{11}(200, t)$ for t= 3, 5, 9, 11) are not very stable.

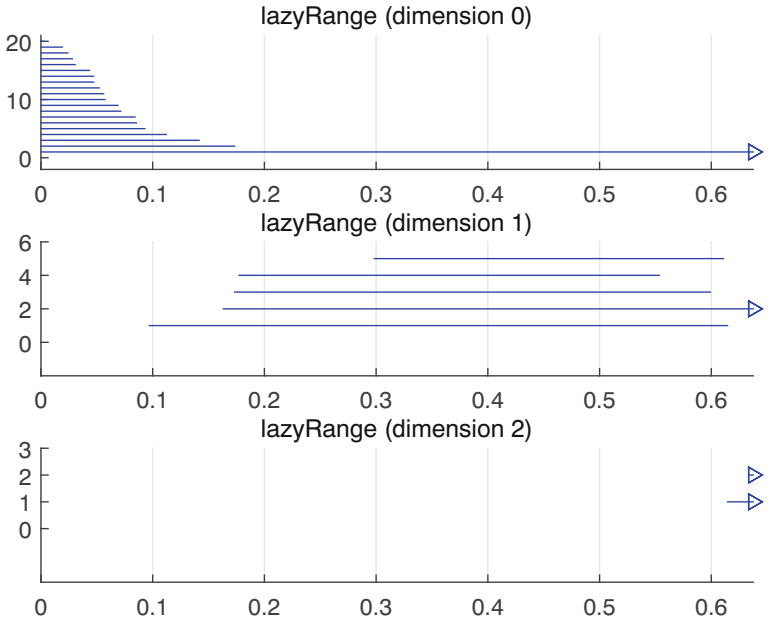

Fig. 32 Barcode results for $CC^9(300)$

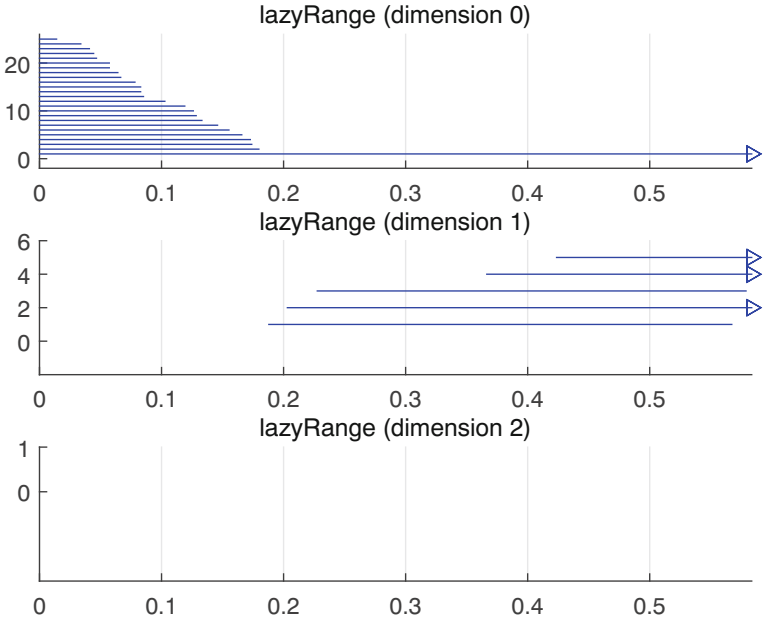

Fig. 33 Barcode results for $CC^{11}(300)$

Remark 2 The author of [19] studied $K^9(140, t)$ for 9×9 range patches and showed that $K^9(140, 9)$ has the same topology as a Klein bottle.

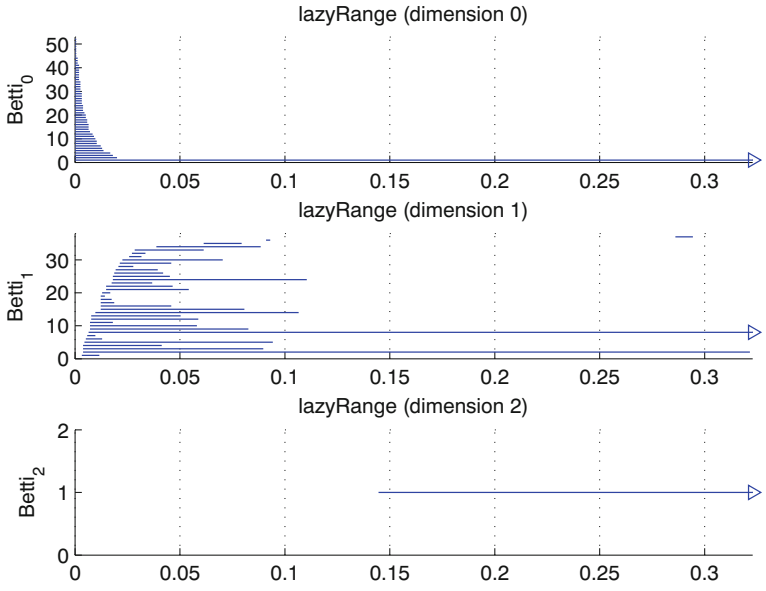

Fig. 34 Barcode results for $K^3(160, 3)$

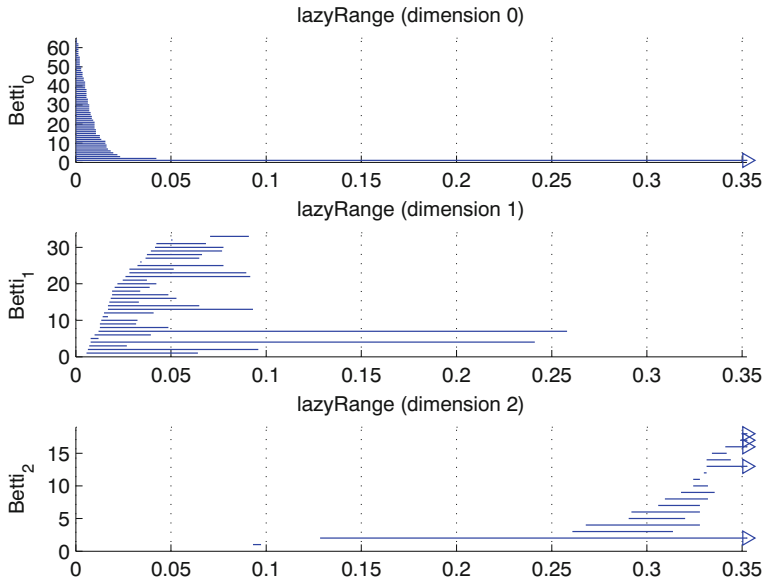

Fig. 35 Barcode results for $K^5(160, 9)$

To discover the largest subspace of M_3 with the same topology as a Klein bottle, we consider $q\%$ of the closest points to $K^3(160)$, which are denoted as $A_q^{(3,160)}$. In [6], Carlsson et al. employed the symbol $A_{0,q}$ to denote the subspace of M acquired by collecting $q\%$ of the nearest points to K_0 and show the subspace $A_{0,50}$ with the homology of a Klein bottle.

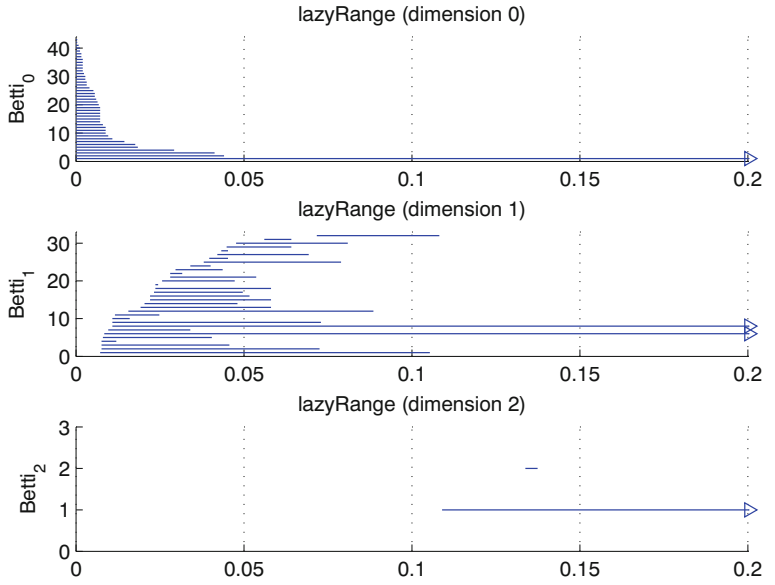

Fig. 36 Barcode results for $K^7(160, 9)$

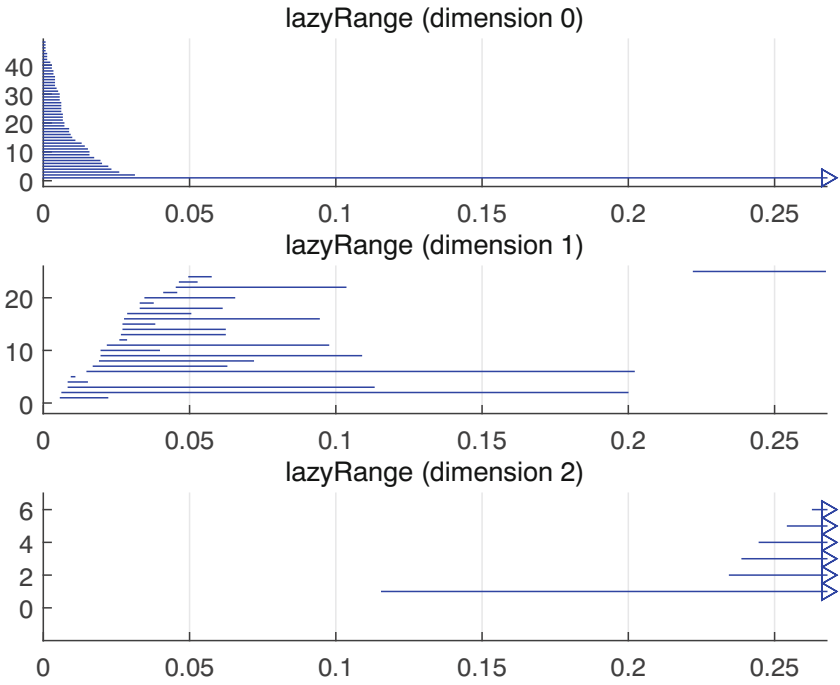

Fig. 37 Barcode results for $K^9(200, 7)$

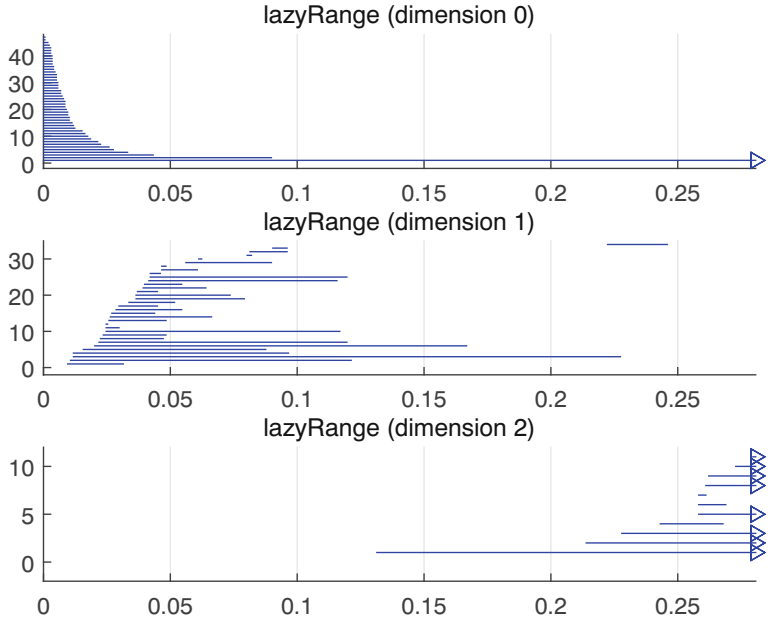

Fig. 38 Barcode results for $K^{11}(200, 7)$

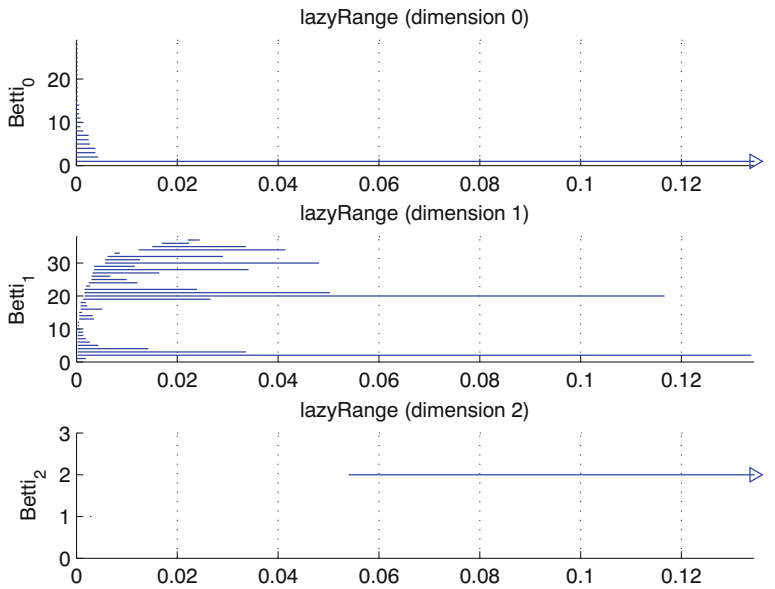

Fig. 39 PLEX results for $A_{28}^{(3,160)} \cup K^3(160, 7)$

However, we cannot determine that the subspace $A_q^{(7,160)}$ has the homology of the Klein bottle for a proper value of q, which shows the difference between optical images and range images.

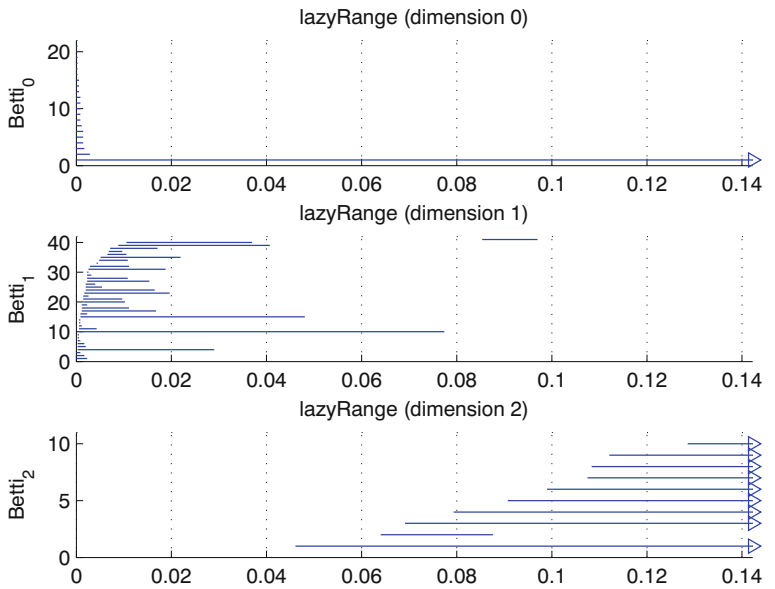

Fig. 40 PLEX results for $A_{33}^{(3,160)} \cup K^3(160, 7)$

Considering the union of $A_{28}^{(3,160)}$ and $K^3(160, 7)$, 121835 points exist in $A_{28}^{(3,160)} \cup K^3(160, 7)$; its size is approximately 29.4% of that of M_3. Figure 39 shows that the subspace can be approximately modeled by a Klein bottle, that is, the largest subspace of M_3 established in this way shows a topological estimation of $K^3(160)$. The topology of the space experiences a change slightly greater than 33%. Figure 40 explains the progress to some extent. Similarly, we consider $A_{20}^{(5,160)} \cup K^5(160, 9)$ ($A_{15}^{(7,160)} \cup K^7(160, 9)$). We observe the existence of the largest subspace of M_5 (M_7) with the topology of the Klein bottle; its size is approximately 20.7% (15.5%) that of M_5 (M_7), which provides a topological approximation to $K^5(160)$ ($K^7(160)$).

For 9×9 and 11×11 range patches, we consider $A_q^{(9,200)} \cup K^9(200, t)$, $A_q^{(11,200)} \cup K^{11}(200, t)$. We perform 2000 experiments for q=5, 7, 8, 9, 10, 11, 12, 13, 15 and t=3, 5, 7, 9, 11. We detect that $A_{11}^{(9,200)} \cup K^9(200, 7)$ ($A_7^{(11,200)} \cup K^{11}(200, 7)$) may be the largest subspace of M_9 (M_{11}) with the homology of a Klein bottle. A total of 32452 (14742) points exist in $A_{11}^{(9,200)} \cup K^9(200, 7)$ ($A_7^{(11,200)} \cup K^{11}(200, 7)$); its size is approximately 11.6% (7.75%) that of M_9 (M_{11}). We perform 200 experiments with $A_{11}^{(9,200)} \cup K^9(200, 7)$, where 154 experimental results show the Klein bottle feature, while the other 46 experiments do not. Figures 41 and 42 present two PLEX results.

Similarly, we perform 100 tests with $A_7^{(11,200)} \cup K^{11}(200, 7)$. We discover that 71 experimental results indicate the homology of a Klein bottle, while the other 29 experiments do not reveal the Klein bottle homology.

The sizes of the largest subspaces of M_m with the topology of the Klein bottle are summarized as Table 1. Thus, we conclude that the Klein bottle feature of the spaces M_3, M_5, M_7, M_9 and M_{11} gradually vanishes as the size of the range patches increases. The author of [18] proves that the largest subspace of 3×3 (5×5, 7×7) natural image patches with

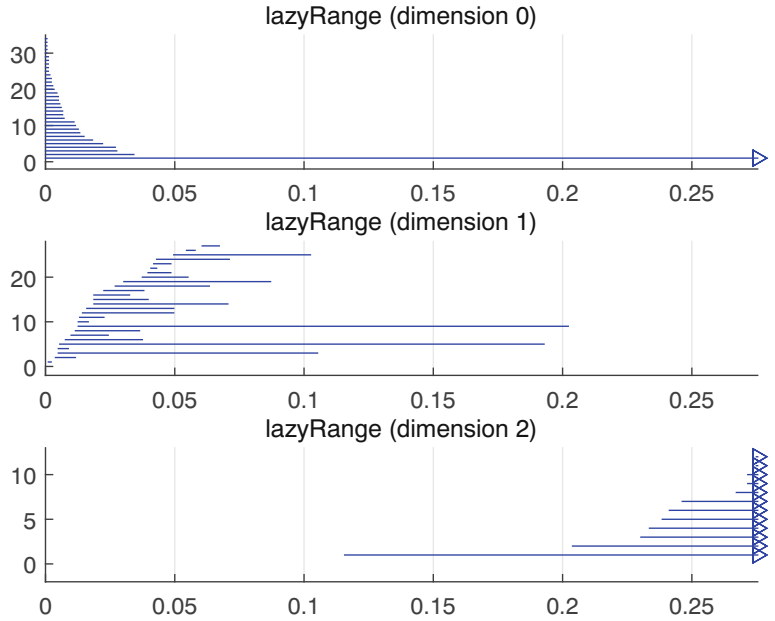

Fig. 41 PLEX results for $A_{11}^{(9,200)} \cup K^9(200, 7)$

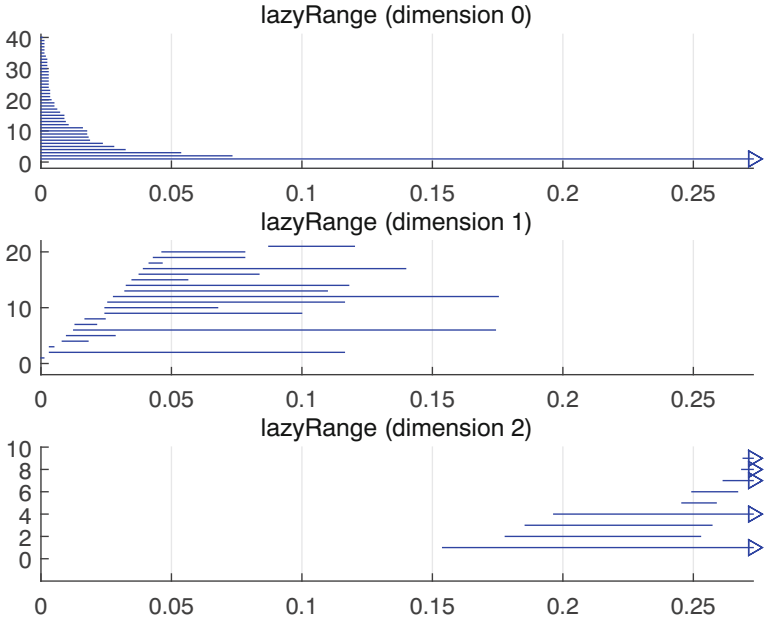

Fig. 42 PLEX results for $A_{11}^{(9,200)} \cup K^9(200, 7)$

the homology of a Klein bottle depends on the measurements of the patches and that its size decreases as the size of the natural image patches increases. Hence, we are usually concerned with the space of $m \times m$ image patches with a sufficiently small m.

9 Conclusions

Topological features of the spaces of 3×3, 5×5, 7×7, 9×9 and 11×11 range image patches are detected by persistent homology. The main advantage of the topological techniques is that they enable the identification of nonlinear properties of the spaces that are potentially difficult to detect by statistical methods. We have shown that the space of 3×3 (9×9 and 11×11) high-contrast range patches has core subsets to be modeled as a circle. By establishing the relationship between the space of range image patches and the space of 2-variable polynomials, we determine that the subspaces of 3×3, 5×5, 7×7, 9×9 and 11×11 patches have the homology of a Klein bottle. These results suggest that the features of the range patches and optical patches are probably similar and that the purpose of image compression by the Klein bottle can be extended to range images.

Acknowledgements The authors are very grateful to the reviewers for valuable comments and corrections. This work was supported by the National Natural Science Foundation of China (No. 61471409).

Compliance with Ethical Standards

Conflict of interests The authors declare that they have no conflict of interest.

References

1. Adams H, Atannas A, Carlsson G (2015) Nudged elastic band in topological data analysis. Topological Methods in Nonlinear Analysis 45:247–272
2. Adams H, Carlsson G (2009) On the nonlinear statistics of range image patches. SIAM J Imag Sci 2:110–117
3. Adams H, Tausz A (2018) Javaplex tutorial, https://github.com/appliedtopology/javaplex
4. Borges M, Vieira A, Carvalho A, D'Angelo M (2020) Local range image descriptor for general point cloud registration. Multimedia Tools and Applications 79:6247–6263
5. Carlsson G (2009) Topology and data. Bulletin (New Series) of the American Mathematical Society 46:255–308
6. Carlsson G, Ishkhanov T, de Silva V, Zomorodian A (2008) On the local behavior of spaces of natural images. Internat J Comput Vis 76:1–12
7. Cha K, Xia S (2018) Nudged elastic band in analysis of range image highcontrast patches. J Phys Conf Series 1098:1–7
8. Edelsbrunner H, Letscher D, Zomorodian A (2002) Topological persistence and simplification. Discrete Comput Geom 28:511–533
9. Field DJ (1987) Relations between the statistics of natural images and the response properties of cortical cells. J Opt Soc Am 4:2379–2394
10. Ghrist R (2008) Barcodes: the persistent topology of data. Bull Amer Math Soc 45:61–75
11. Hatcher A (2002) Algebraic topology. Cambridge University Press, Cambridge
12. Huang J, Lee A, Mumford D (2000) Statistics of range images. In: Proc of IEEE conf on computer vision and pattern recognition, Hilton Head Island, SC, pp 324–331
13. Idrobo-Pizo G, Motta J, Borges D (2019) Novel invariant feature descriptor and a pipeline for range image registration in robotic welding applications. Iet Image Process 13:964–974
14. Jung S, Song S, Chang M, Park S (2018) Range image registration based on 2D synthetic images. Computer-aided Design 94:16–27
15. Lee AB, Pedersen KS, Mumford D (2003) The non-linear statistics of high-contrast patches in natural images. Internat J Comput Vis 54:83–103
16. Roth S, Black MJ (2007) On the spatial statistics of optical flow. Internat J Comput Vis 74:33–50
17. Shen Y, Wang J, Lindenbergh R, Hofland B, Ferreira VG (2018) Range image technique for change analysis of rock slopes using dense point cloud data, Remote Sensing, vol. 10 10.3390/rs10111792
18. Xia S (2016) A topological analysis of high-contrast patches in natural images. J Nonlinear Sci Appl 9:126–138
19. Yin Q (2015) On qualitative analysis of high-contrast patches in range images, presented at the. In: Wong W (ed) Proceedings of the 4th international conference on computer engineering and networks. lecture notes in electrical engineering, vol 355. Springer, Cham, pp 573–582
20. Zomorodian A, Carlsson G (2005) Computing persistent homology. Discrete Comput Geom 33:249–274
21. de Silva V, Carlsson G (2004) Topological estimation using witness complexes. In: Proceedings of the first eurographics conference on point-based graphics, Switzerland, pp 157–166
22. van Hateren JH (1992) Theoretical predictions of spatiotemporal receptive fields of fly LMCs, and experimental validation. J Comp Physiol A 171:157–170

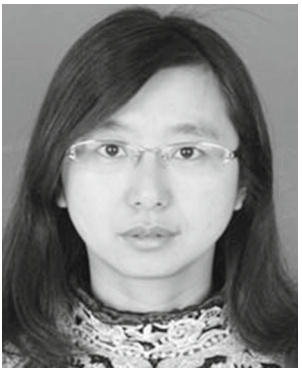

Jinhong Li

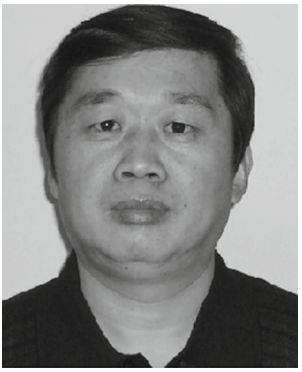

Shengxiang Xia